Journal of Materials Chemistry A

Accepted Manuscript

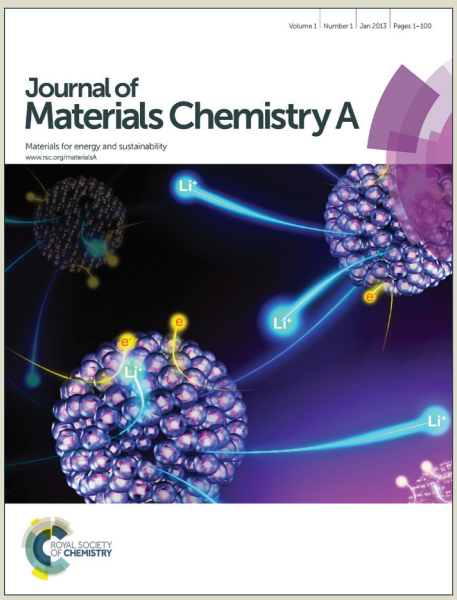

ROYAL SOCIETY OF CHEMISTRY

www.rsc.org/materialsA

Journal of

Materials Chemistry A

RSCPublishing

ARTICLE

A High Energy Density Azobenzene/Graphene Hybrid: A Nano-Templated Platform for Solar Thermal Storage

Cite this: DOI: 10.1039/x0xx00000x

Received 00th February 2015,
Accepted 00th 000000o 2015

DOI: 10.1039/x0xx00000x

www.rsc.org/

Wen Luo,[a] Yiyu Feng,[a] Chen Cao,[a] Man Li,[a] Enzuo Liu,[a] Shipei Li,[a] Chengqun Qin,[a] Wenping Hu[b] and Wei Feng*[a]

Effective conversion of light into heat is an emerging field of a great potential for large-scale application, markedly driven by novel molecules and structures. Unfortunately, until now, it is still hindered by a low storage capacity and short-time storage. A nano-template of covalently attaching new azobenzene chromophores on graphene as solar thermal fuels were present here, in which intermolecular hydrogen bond and proximity-induced interaction, resulting from high functionalization density and inter-planar bundling interaction, remarkably improve both storage capacity and lifetime. This nanoscopic template exhibits a high energy density up to 112 Wh kg^{-1} and a long-term storage with a half-life of more than one month (33days), which is also confirmed by the calculation using density functional theory, simultaneously keeping an excellent cycling stability tuned by visible light for 50 cycles. Our work develops a promising class of solar thermal fuels with high energy density, which outperform previous nano-materials and are comparable to commercial soft-packing Li-ion batteries.

Introduction

Chemical strategy for utilizing the environmentally clean and abundant energy from sunlight receives great attention as a means of efficiently capturing, converting and storing solar energy in the form of chemical bonds.[1,2] Recently, a new pathway for storing energy has been explored. Solar thermal fuels, with metastable forms capable of releasing close to 100% stored energy as heat source under the external stimulus along with the reversion to stable forms, are regarded to be a closed-cycle system that only transfers energy from and to the environment by reversible transformation.[3] Moreover, thermal storage of sunlight in rearranged chemical bonds opens a gate for developing a large-scale utilization of solar-energy in a convenient form of liquid or powder without the emission of greenhouse gas (CO_2). However, solar thermal fuel is still not an applicable solution due to a low storage capacity, low thermodynamic stability and irreversible degradation at a long-time irradiation limited by molecules.[4-6] Thus, the development of building novel structural materials or templates based on the molecular design is critically important for advanced solar thermal fuels.

Azobenzene chromophores (AZO), of great interest for numerous applications,[7-11]have been considered as one of the most attractive compounds for solar thermal fuels[3] owing to its good light-response, reversible isomerization and tunable thermal reversion. However, it remains a great challenge to meet the requirement of solar thermal fuels because of a quite low energy density and a short storage half-life ($\tau_{1/2}$, the time required for the quantity of *cis*-isomer to fall to half its value by the reversion) of a single molecule mainly caused by a low ΔH (energy difference between *trans*- and *cis*-isomers) and ΔE_a (thermal barrier for the reversion process).[12] However, these problems can be potentially overcome by azobenzenes/carbon nanostructure hybrids based on the multiple molecular interactions and tunable steric configuration. Grossman *et al*[13] predicted that the storage capacity and stability of AZO/carbon nanotube (CNT) hybrids were remarkably improved by multi-intermolecular interactions between neighboring AZO molecules on the surface of CNT based on the calculation using density functional theory. This calculation is also supported by a series of other AZO/carbon nanostructures with a quite high theoretical energy density and long-term storage by optimizing

intermolecular interactions.[3] Results indicate that molecular interactions such as hydrogen bonds (H-bonds) and proximity-induced interaction could significantly increase ΔH and $\tau_{1/2}$ for per AZO molecule, resulting in an increase in storage capacity and storage stability for solar thermal fuels. However, molecular interactions in the previous calculations are mainly determined by suitable intermolecular distance and steric configuration of AZO on carbon nano-templates based on high functionalization densities[13]that combine the increasing number of intermolecular interaction per unit volume and enhanced storage capacities per unit weight, resulting in a long-term and high energy density of solar thermal storage.

Unfortunately, the energy densities of existing AZO/carbon nanomaterials[14,15] for solar energy storage are still lower than that of soft-packing Li-ion batteries (90~150 Wh kg^{-1})[16]. These low storage capacities mainly arise from a low ΔH for single AZO with a low functionalization density 1/40~80 [17-19] (each AZO supported by 40~80 carbon atoms) compared with that in theoretical models (1/4~8). As a results, the increasing number of molecular interaction and high functionalization density in AZO/carbon nano-template are essentially important to enhance energy density and storage lifetime of solar thermal fuels.

In this work, we designed a nano-template of solar thermal fuels with high functionalization density composed of AZO molecules with methoxyl and/or carboxyl groups covalently attached on the surface of graphene nanosheets, as shown in Fig. 1. Furthermore, we demonstrated that this nano-template for solar energy storage achieves a high storage capacity (112 Wh kg^{-1}) and a long-term storage lifetime ($\tau_{1/2}$ of 33 days) using intermolecular H-bonds and proximity-induced interaction owing to the high functionalization density and solid-state inter-planar bundling with packing interaction. Results also indicate that solar thermal fuels show a robust cycling performance for 50 cycles, affording a long utilization of at least 4.5 years.

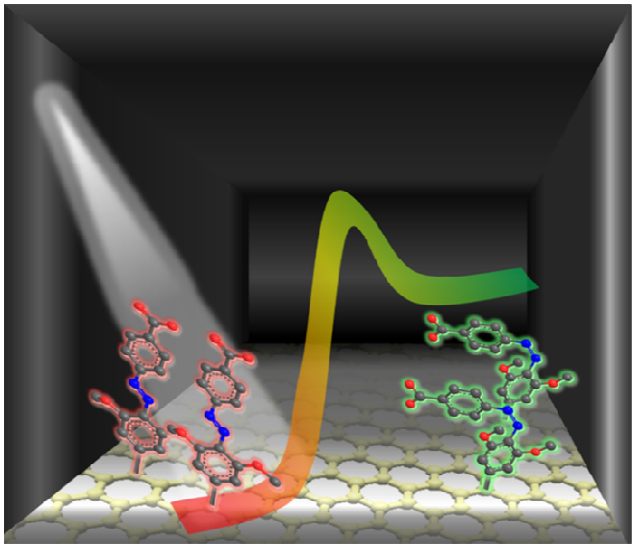

Fig.1 Schematic illustration of AZO-RGO hybrid for solar thermal storage. Energy from sunlight can be stored in the form of chemical bonds by photochemically-induced *trans*-to-*cis* transformation and be released as heat source tuned by *cis*-to-*trans* reversion.

Experimental

Synthesis of RGO, AZO molecules and RGO-AZO.

GO was prepared through the acid oxidation of flake graphite according to the literature[20]. GO solution in water (150 mL, 1 mg mL^{-1}) was adjusted to pH ~ 9 with 5 wt% sodium carbonate solution, and the partial reduction of GO was carried out using 30 mL sodium borohydride solution (20 mg mL^{-1}) at 85℃ for 2h. Then RGO was obtained after centrifugation, filtration and rinsing with distilled water for several times. The resultant RGO was re-dispersed in distilled water at the concentration of 1mg mL^{-1} by mild ultrasonication.

Typically of AZO-1: aniline (0.91 mL, 10 mmol) and $NaNO_2$ (0.69 g, 10 mmol) were dissolved in 40 mL distilled water, and the mixture was slowly added into HCl solution (40 mL, 1 mol L^{-1}) in an ice bath at 0~5℃ for the diazotization. The generated diazonium salt solution was then slowly added into the suspension of 3,5-dimethoxyaniline (1.53 g, 10 mmol) at pH of 6~7 at 0~5℃ for 4 hours under argon. The resultant raw materials was filtered and purified by chromatography on silica with N-hexane/ethyl acetate as eluent and the final solid was 1.59 g (Yield: 62 %). ^{1}H NMR (500 MHz, DMSO-d_6, δ): 7.69 (d, 2H, Ar-H), 7.46 (t, 2H, Ar-H), 7.27 (t, 2H, Ar-H), 6.15 (s, 1H, Ar-H), 4.06 (s, 2H, N-H), 3.80 (s, 6H，O-CH_3). HRMS (m/z): [M]+ calcd. for $C_{14}H_{16}N_3O_2$, 258.1237; found, 258.1232; analysis (calcd., found for $C_{14}H_{16}N_3O_2$): C(65.10,65.02), H(6.24,6.26), N(16.27,16.27), O(12.39,12.45). AZO-2 was also synthesized by coupling reaction using 4-aminobenzoic acid and 3, 5-dimethoxyaniline by a similar method and the final solid was 1.71g (Yield: 57%). ^{1}H NMR (500 MHz, DMSO-d_6, δ): 12.55 (s, 1H, COOH), 8.02 (d, 2H, Ar-H),7.95 (d, 2H, Ar-H), 7.22 (s , 2H, Ar-H), 4.01 (s, 2H, N-H), 3.82 (s, 6H, O-CH_3). HRMS (m/z): [M]+ calcd. for $C_{15}H_{16}N_3O_4$, 302.1135; found, 302.1131; analysis (calcd., found for $C_{15}H_{16}N_3O_4$): C (59.60,59.53), H (5.33,5.35), N (13.90,13.90), O (21.17,21.22).

RGO-AZO nano hybrids were obtained by covalently functionalized AZO molecules on RGO surface via aryl radicals according to the literature[21] with some modifications. Typically of AZO-2-RGO: AZO-2 molecule (1.204 g, 4 mmol) and $NaNO_2$ (0.276 g, 4 mmol) were dissolved in 40 mL di-water at room temperature, and then was slowly added to HCl solution (20 mL, 1 mol L^{-1}) in an ice bath to form diazonium salt in one hour. This diazonium salt solution was slowly dripped into the above typical RGO solution (100 mL, 1 mg mL^{-1}). The reaction was carried out for 4 hours at 0~5℃ and kept at room temperature overnight. The mixture then was washed with distilled water, acetone and DMF for several times to remove the remaining AZO-2 molecule and excessive diazonium salts by the filtration using polytetrafluoroethylene (Teflon) membrane. The resulting solid was collected until the filtrate showed no characteristic absorption band in UV-Vis spectra. This functionalization was repeated for two times with a half molar quantity to increase functionalization density. Finally, AZO-2-RGO was attained after dry in vacuum overnight at 70℃. AZO-1-RGO was also prepared by a similar method for the comparison.

Characterization.

Fourier transform infrared (FTIR) spectra were recorded on a Bruker Tensor 27 spectrometer with a disc of KBr. ^{1}H NMR spectra were carried out on a Varian INOVA 500 MHz spectrometer with trimethylsilyl as an internal standard. Chemical shifts were referenced to the solvent values (δ= 2.49 ppm for DMSO-d_6). X-ray (1250 eV) source at a base pressure in the 10^{-8} to 10^{-9} Torr range. X-ray diffraction (XRD) patterns were taken by a Rigaku D/max 2500 v/pc X-ray diffractometer using Cu Ka radiation (k=0.15 nm) at a scanning rate of 8.0°/min, a voltage of 40 kV and a current of 200 mA. Thermal analysis was studied using a Thermogravimetric Analyzer Instrument (TGA, NETZSCH STA 449C). The samples were heated from 30 to 800℃ at a rate of 5℃/min in an aluminum

crucible under 50 mL/min of nitrogen purging. X-ray photoelectron spectroscopy (XPS) analysis was performed on a PHI 1600 model surface analysis system with a 450 W Mg Ka. Transmission electron microscope (TEM, Phlilps Tecnai G2 F20 at 200 kV) and scanning electronic microscope (SEM, Hitachi S-4800) were performed to observe the morphologies. High-resolution mass spectrometry （HRMS） was carried out on a Bruker Daltonics APEXIV 4.7 T Fourier Transform Ion Cyclotron Resonance Mass Spectrometer.

Time-evolved UV-Vis absorption spectra of AZO and AZO-RGO hybrids in DMF solution using 1 cm path length quartz cuvettes were recorded using a Hitachi 330 UV-Vis spectrophotometer. *Trans*-to-*cis* isomerization process of AZO molecules and AZO-RGO hybrids were irradiated by mercury lamp (Beijing Changtuo Technology Company) at 500 W with a filter set of 365 nm, as a light source positioned at 20 cm distance to the samples at room temperature. *Cis*-to-*trans* thermal reversion process was investigated using UV-Vis spectrophotometer after the storage in darkness covered by foils or irradiated by visible light at 540 nm at room temperature while the rate of thermal reversion was calculated based on a change in intensity of transition bands of AZO on RGO.

Energy density of AZO and AZO-RGO were determined using differential scanning calorimetry (Perkin Elmer Diamond DSC). For AZO-2, a typical process was shown as following: AZO-2 solution (100 mg mL^{-1}, 4 mL) in acetonitrile was added in a cuvette. The cuvette was sealed and then irradiated with UV light at 365 nm (25°C) until the intensity of absorption band shows no change, indicating that PSS was reached (almost all is *cis*- isomer). The irradiation was stopped and the sample was transferred via foil-wrapped syringe to a foil-wrapped agate mortar where it was concentrated to dryness in vacuum while avoiding isomerization from *cis* to *trans* under the light. The solid powder was immediately transferred into the pan. Then the pan was hermetically sealed and re-weighed. Samples were analyzed by DSC with the following method: Equilibration at 10°C, heating to 180°C at 5°C/min for calculating heat release in reversion from *cis* to *trans* isomer. Cooling down to 10 °C at 5°C/min and re-heating to 180°C at 5°C/min as a comparison without heat flow, indicating the heat release in first heating was stored energy from the light.

Model and calculation.

Our total energy and electronic structure calculations were performed using the projector augmented wave (PAW) formalism of density functional theory as implemented in the Vienna ab initio Simulation Package (VASP)[22] is used in the system energy and electronic structure calculations. The energy cutoff for plane-wave expansion of the PAW's is 400 eV. The exchange-correlation functional is approximated with the generalized gradient approximation proposed by Perdew, Burke, and Ernzerhof (PBE)[23]. The Gaussian smearing method[24] was used and the width of smearing was chosen as 0.05 eV. For geometry optimizations, all the internal coordinates are relaxed until the Hellmann-Feynman forces are less than 0.03 eV/Å. According to the experimental results by TGA and XPS characterization, the supercell of graphene nano-ribbons containing 40/32 carbon atoms for AZO1-RGO and AZO2-RGO respectively was used and separated by a vacuum region of more than 20 Å along the y-axis and 15 Å along the z-axis. The Brillouin zone is sampled using Monkhorst-Pack scheme [25]with 1×1×1 and 3×1×1 k-point grid for geometry optimization and system energy calculations, respectively.

Results and discussion

Design and preparation of AZO-RGO nano-template.

An excellent nano-template for regulating the storage capacity and stability of solar thermal fuels is high density of locally rigid chromophore molecules covalently attached on low-mass nanostructures for intra- and/or intermolecular interactions. Reduced graphene oxide (RGO) is regarded as an ideal nanostructured platform to support photoactive molecules for close-packed and ordered arrangement based on a high functionalization density owing to the combination of partial restoration of conjugated structures and good dispersion in water. What is more, enhanced intermolecular interactions[13] (such as H-bonds and proximity-induced interaction) between neighboring AZO molecules on the surface of RGO can be attained by a variety of substituent groups on the benzene ring and steric configuration with decreasing distance. The intermolecular interactions significantly improve the storage capacity for solar energy storage with high functionalization density. Previous investigations[14] also demonstrated that AZO/RGO hybrid showed a great potential for a high storage capacity, that is higher than AZO/single-walled carbon nanotubes (SWCNT)[15] hybrid at a similar functionalization density. Furthermore, as shown in Fig. 2, the amount of stored energy can be further improved by optimizing the molecular structure and packing interaction (bundling) of AZO on neighboring nanosheets. This bundling effect is critical for optimizing molecular interaction and steric configuration of AZO-RGO template for solar thermal storage.

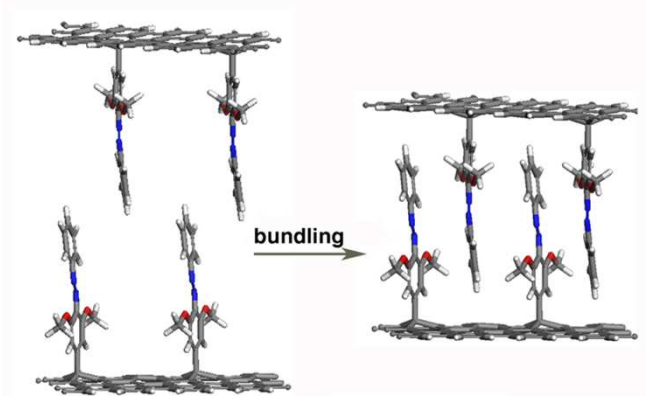

Fig.2 Mechanism illustration of inter-planar bundling for high functionalization density AZO-RGO hybrids that in the solution (left) AZO-RGO hybrids show no packing interaction because of a large interlayer spacing , while show packing interaction in the solid state forms due to the bundling with a low interlayer space (right).

Here, we synthesized two molecules (Fig. S1†), 4-((3,5-dimethoxyaniline) diazenyl)-benzene (AZO-1) and 4-((3,5-dimethoxyaniline) diazenyl)-4-benzoic acid (AZO-2), which are covalently functionalized with RGO for solar thermal fuels. Two methoxy groups in ortho-position of two AZO molecules enable molecular interaction and steric hindrance. Besides, -COOH in para-position of AZO-2 forms intermolecular H-bond and proximity-induced interaction controlled by steric configuration and specific intermolecular distance. Thus, high functionalization density of AZO on RGO is significantly important for enhancing molecular interaction and steric hindrance during the transformation. However, the increase in functionalization density of AZO-RGO is restricted by the decreased reactivity, steric hindrance of AZO and the stacking of nanosheets. This analysis is confirmed by the experiment that the functionalization density is about 1/40 (Table S1 †) after only once functionalization, and that, it is far from desired functionalization density for solar thermal fuels.

In this study, we utilized a triple iterating reaction using aryl radicals[21,26,27] (Fig. S2†) to increase functionalization density up to 1/16~19 (Table 1, detail disscus later) by increasing collision probability, reactivity and template-substrate interaction. High functionalization density favors the inter-layer bundling of solid-state AZO-RGO further decreasing intermolecular distance and increasing intermolecular interaction for high storage capacity and good stability. Moreover, it is worth mentioning that the AZO-RGO hybrids show well-dispersion in polar organic solvents including acetone, N,N-dimethylformamide (DMF) and acetonitrile (> 1 mg mL-1) without any precipitate for several months (Fig. S3).

Morphologies and chemical structures of AZO-RGO nano-template.

Morphologies of RGO and AZO-RGO hybrids were observed by TEM. The nanosheets of RGO (Fig. 3a and 3b) are wrinkled with a slightly rough surface, and simultaneously the crystal lattice of RGO retains its clear hexagonal pattern after reduction according to corresponding fast fourier transforms (FTTs, the inset of Fig. 3b). However, the crystal lattice of AZO-RGO retains its hexagonal pattern but not clear enough (Fig. 3c, 3d and the inset of Fig. 3d) after only once functionalization due to a low functionalization density. As shown in Fig. 3e and 3f, the rough surface of dispersed nanosheets appears to be covered by the addends after a triple iterating functionalization. The formation of orderly distributed domains of immobilized AZO in the region of local place simultaneously affects the crystal lattice of the flakes in FTTs pattern[27], manifesting non-hexagonal gpattern (the inset of Fig. 3f). This microstructure is different from that of non-covalently functionalized graphene with some organic molecules[28], indicating a high functionalization density of AZO on RGO confirmed by the result of TGA and XPS further discussion below. Besides, we have observed orderly stacked nanosheets in the solid state by SEM (Fig. S4†), which favors the inter-layered bundling that can further enhance intermolecular interactions among AZO on the surface of nanosheets.

Here we demonstrate the covalent linkage of AZO attached to RGO supported by FTIR spectra (Fig. 4c and Fig. S5†) and XPS (Fig. S6 and S7†). Both AZO-1-RGO and AZO-2-RGO exhibit two new bands at ~ 2959 cm^{-1} and 2874 cm^{-1} assigned to -OCH_3 stretching mode and a band at 1394 cm^{-1} corresponding to N=N stretch after the attachment. Furthermore, a broad band at 3412 cm^{-1} and the peak at 1630 cm^{-1} in AZO-2-RGO are attributed to -OH and -C=O stretching of COOH in the para-substitution, respectively. Besides, compared with AZO-2 (1690 cm^{-1} and 3490 cm^{-1}, Fig. S5), a large red-shift of C=O and O-H stretching of -COOH indicates the formation of the intermolecular H-bonds of OH---O between two adjacent AZO on RGO.[29,30] Moreover, we also confirmed the covalent linkage by C1s and N1s XPS (Fig. S6†) that the N1s region of AZO-RGO hybrids show only one band of -N=N- (and/or N-C) at 400 eV[31] without the characteristic peak of -NH_2 at 401.5 eV[32] on the shoulder.

We provide the further details about the analysis of high functionalization density of AZO-RGO by TGA (Fig. 4a and 4b) and XPS (Fig. S7†). RGO exhibits a good thermal stability and its weight loss is the elimination of remaining oxygen groups. AZO-1 (AZO-2) is thermally stable from 30 to 240℃(230℃)

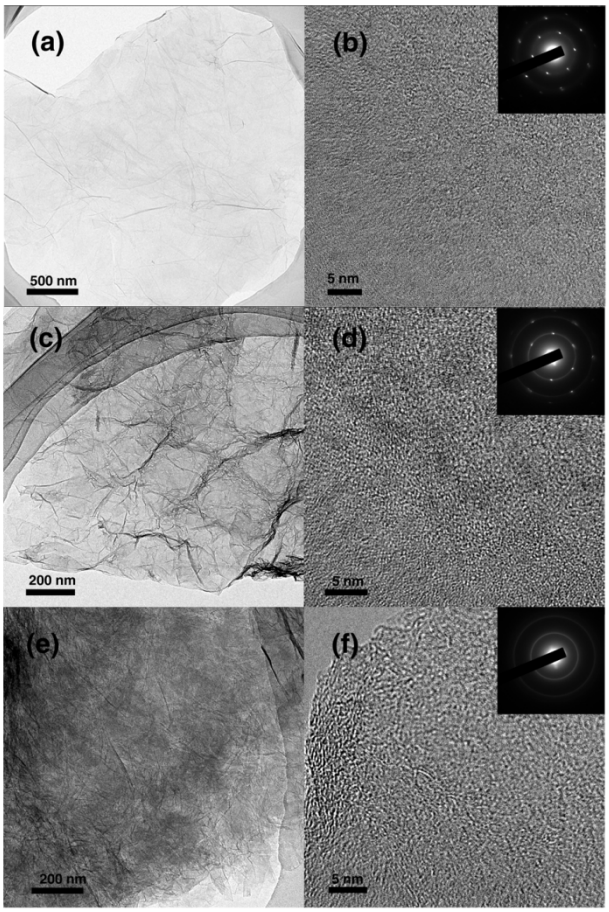

Fig.3 TEM with a high-resolution image and the inset of FTTs pattern of (a) and (b) RGO, (c) and (d) AZO-RGO hybrid (low functionalization density) prepared by only once functionalization, (e) and (f) AZO-RGO hybrid (high functionalization density) prepared by triple iterating functionalization.

and subsequently shows a sharp weight loss between 240 and 330℃ (230 and 350℃) with slow loss from 330 (350) to 800℃.Thermal decomposition temperatures of two AZO are slightly increased by the covalent attachment on RGO in comparison of pure AZO. Thus, the weight loss of AZO-RGO arises from the elimination of remaining oxygen groups of RGO and the decomposition of AZO with two stages. Here, we defined the bulk-average functionalization density ($\boldsymbol{D_f}$) as the average number of carbon atoms support one AZO that can be calculated based on the grafting degree ($\boldsymbol{D_g}$) at three different temperatures (600℃, 700℃ and 800℃) according to the Equation (1)[33] shown in Table 1. Wherein, Rg, R and Ra represent the residual weight percentage (wt%) of RGO, AZO and AZO-RGO, respectively.

$$D_g(\%) = \frac{R_g - R}{R_g - R_a} \times 100\% \quad (1)$$

Table 1. Functionalization densities of AZO on RGO calculated by TGA and XPS

	TGA				XPS		
	D_g (%)			D_f	Element content (%)		D_f
	600	700	800		C	N	
RGO	80.15	75.81	71.76	/	85.6	/	/
AZO-1-RGO	48.85	48.84	48.83	1:19.0	77.2	4.6	1:19.6
AZO-2-RGO	57.26	57.30	57.24	1:16.4	74.7	4.8	1:16.1

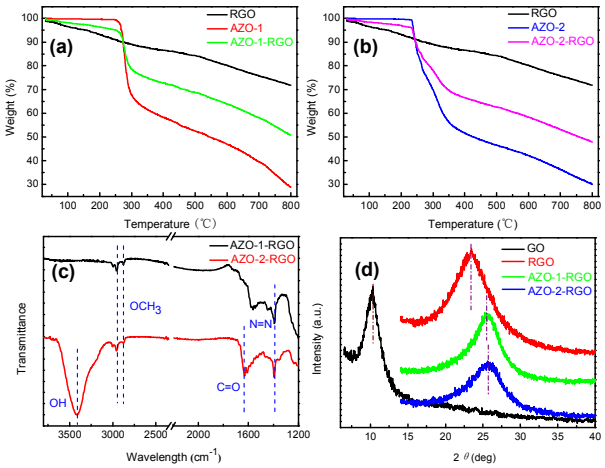

Fig.4 Characterization of high functionalization density AZO-RGO. (a) TGA of RGO, AZO-1 and AZO-1-RGO. (b) TGA of RGO, AZO and AZO-RGO. (c) FTIR spectra of AZO-RGO in the region of 1200-3800 cm-1. (d) XRD of GO, RGO and AZO-RGO.

In particular, the functionalization density also could be estimated by element composition data in XPS[34] based on atomic percentage of the emerging nitrogen shown in Table S1 and Table 1. Specifically, the density is 1/19 by a triple iterating reaction for AZO-1-RGO comparing 1/40 by once functionalization, while 1/16 is obtained for AZO-2-RGO comparing 1/38 by once functionalization. The above results indicate that one AZO is approximately covalently supported by per 16~19 carbon atoms of RGO by a triple iterating functionalization, which is comparable to or higher than that in previous studies[17-19,35].

On the other hand, we have found that AZO-RGO shows a shift of G band to 1584 cm^{-1} with a slight increase in D/G ratio compared with pure RGO (1595 cm^{-1}) due to an increasing covalent functionalization of AZO on the nanosheets[36] shown in Raman spectroscopy (Fig. S8†). This founding is the direct evidence for the frequent introduction of sp^3-hybridized carbon atoms into the sp^2-hybridized graphene layers because of the covalent attachment of AZO molecules on RGO. What is more, the disappearance of 2D resonance at 2698 cm^{-1} related to packing interaction as well as the overall broadening of the line widths comparable to RGO further indicated the high functionalization density of AZO-RGO.[27] Meanwhile, a slight shift of 2θ peaks of AZO-RGO (AZO-1-RGO at 25.6° and AZO-2-RGO at 25.8°) compared with RGO (23.5°) in XRD (Fig. 4d) is attributed to the inter-planar bundling of nanosheets in the solid state, consistent with TEM (Fig. 3) and SEM (Fig. S4†) observation in the previous section. We stress that this bundling effect results in close intercalation, which remarkably increases the storage capacity and lifetime of the solar thermal fuels.[15,37,38]

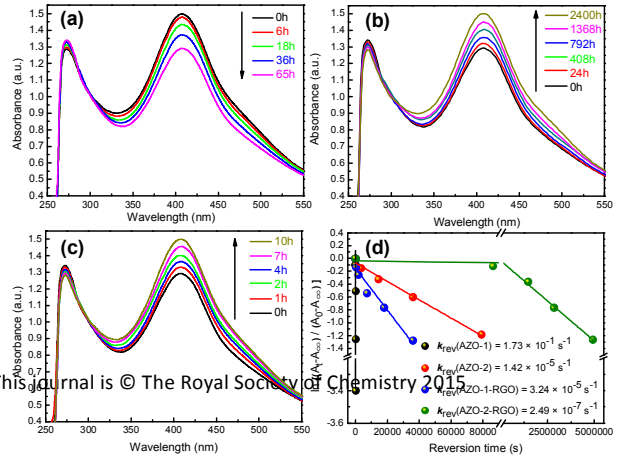

Fig.5 Time-evolved absorption spectra of AZO-2-RGO with an initial absorbance intensity of 1.5 arbitrary unit (a.u.) at room temperature (25℃). (a) Irradiated by UV light at 365 nm, (b) in darkness and (c) irradiated by visible light at 540 nm. (d) First plots of *cis*-to-*trans* thermal reversion of AZO and RGO-AZO hybrids with different k_{rev} (the inset).

Photoisomerization and long-term reversion of AZO-RGO. As shown in Fig. 5, we investigated the isomerization and reversion of AZO and AZO-RGO in DMF (0.1 mg mL^{-1}) using UV-Vis absorption spectra controlled by the change of electronic transition. First, we irradiated the samples by UV light at 365 nm to a photostationary state (PSS), and then recorded the reversion in darkness or irradiating by 540 nm visible light. Relative to the maximum peak at 398 nm in AZO-1-RGO, AZO-2-RGO shows a red-shifted π-π* transition band with the maximum peak at 408 nm because of a push-pull molecular structure. Electron transitions in visible region of AZO-RGO favor the thermal fuels can sufficiently absorb solar power that is very important for large-scale application. Moreover, both AZO-1-RGO (Fig. S9a†) and AZO-2-RGO (Fig. 5a) show a continuous decrease in π-π* transition band due to *trans*-to-*cis* isomerization of AZO appended on RGO until PSS is generated, but the rate of the isomerization is relatively lower than that of pure AZO (Fig. S9c† and S9e†). Likewise, we found AZO-RGO hybrids (Fig. 5d) after the irradiation reveal an appreciably slow thermal *cis*-to-*trans* reversion with the first-order rate constant several orders of magnitudes lower than that of pure AZO according to according to the Equation (2)[14]. Wherein, A_0 is the absorption intensity of AZO at a photostationary state between *trans*- and *cis*-isomers after the irradiation, A_t is the absorption intensity of AZO kept in darkness or irradiated by visible light for a "t" time, A_∞ is the absorption intensity of AZO after the complete *cis*-to-*trans* reversion.

$$\ln(\frac{A_\infty - A_t}{A_\infty - A_0}) = -k_{rev}t \quad (2)$$

Furthermore, we were delighted to find that AZO-2-RGO exhibits a long-term spontaneous reversion with a $\tau_{1/2}$ of metastable isomer up to 792 h at room temperature and energy can be completely released in about 100 days (Fig. 5b). In other word, AZO-2-RGO spontaneously releases a half amount of solar thermal energy for more than one month (33 days) that would allow it to be utilized for long-term solar thermal storage[38] attributed to intermolecular H-bonds (consistent with FTIR spectra) and steric hindrance of AZO on RGO controlled by a high functionalization density (1/16~19 in average). Meanwhile, the decreased average intermolecular distance between neighboring AZO on the surface of nanosheets at high functionalization density avails intermolecular interactions based on oriented steric configuration to obtain a higher energy density.[3]

A tunable solar thermal storage.

Although a slow reversion reduces the loss of heat during the storage, the release of heat controlled by external effects (light, heat or chemicals) at different times or environment is of great importance for the application of AZO-RGO as solar thermal fuels. As shown in Fig. 5c, under the irradiation of visible light at 540 nm (a power density of 20 mW cm^{-2}), AZO-2-RGO shows a much faster *cis*-to-*trans* reversion than that in darkness indicated by a continuous increase in n-π* transition band similar to the reversion accelerated by high-temperature. And we demonstrated that the first-order rate constants of the reversion of AZO-2-RGO induced by visible light or high-temperature (85 ℃) (Fig. S10†) are two and five order of magnitude higher than that of spontaneousin reversion in the darkness at room temperature (Fig. 5d), respectively. This accelerated reversion of *cis*-to-*trans* transformation is because of the fact that metastable AZO on RGO absorb a certain amount of energy from light or heat[39-42], which is high enough to surmount thermal barrier (ΔE_a). Moreover, the intensity and wavelength of visible light and the different temperatures can easily tuned the reversion that enable the release of solar heat at different rates. We point out that the photo- or heat-induced reversion is crucial for the potential application of solar thermal fuels using AZO-RGO nano-templates.

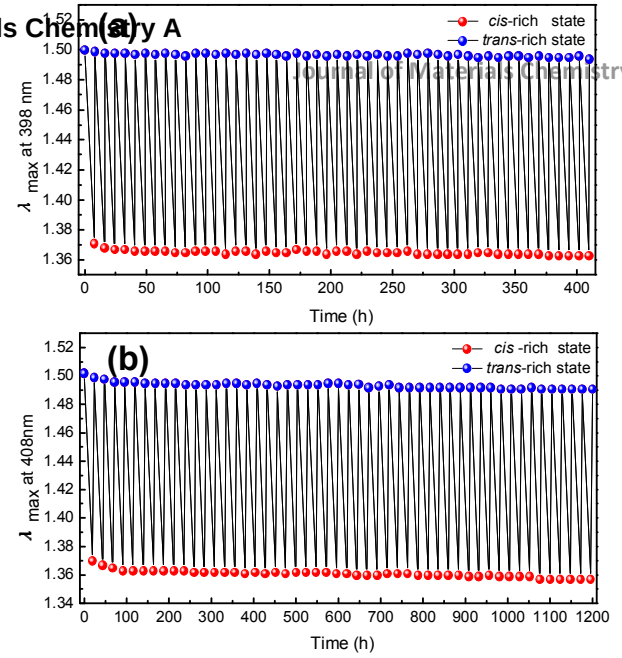

Fig.6 Cycling stability of AZO-RGO by an alternative irradiation by UV and visible light for 50 cycles. (a) Absorbance of AZO-1-RGO at 398nm was recorded after the irradiation at 365 nm and 540nm for 8 h and 12 min. (b) Absorbance of AZO-2-RGO at 408 nm was recorded after the irradiation at 365 nm and 540nm for 20 h and 4 h.

We further investigated cycling stability of AZO-RGO nano-template by the *trans-cis-trans* isomerization for a long-term storage.The samples were irradiated by UV light at 365 nm at a low power density (20 mW cm^{-2}) until a *cis*-rich state, and they are immediately irradiated by visible light at 540 nm (20 mW cm^{-2}) to reverse a *trans*-rich state. Fig. 6 showed the absorbance of the *trans*-rich and *cis*-to-*trans* after different irradiation, indicating that AZO-RGO show an excellent stability of isomerization and reversion for 50 cycles without the degradation similar to that of pure AZO for 100 cycles (Fig. S11†) for storage and release of heat energy. And that, this excellent cycling stability of solar thermal fuels using AZO-RGO nano-template is also confirmed by the spontaneous reversion in darkness (25 ℃) without any precipitate after irradiation (Fig. S3†). To recap, above results demonstrate that AZO-2-RGO can be developed for long-term utilization as solar thermal fuels with the stability up to 4.5 year (33 days for a $\tau_{1/2}$ × 50 cycles).

Table 2. Bulk energy densities of AZO-RGO measured by DSC and calculated by DFT

	M_n[(a)] g mol^{-1}	Calculation Wh kg^{-1}	Measurement Wh kg^{-1}	$\Delta H_{cis\text{-}trans}$ KJ mol^{-1}
AZO-1	257	47.97	42.04	38.90
AZO-2	301	41.86	40.52	43.92
AZO-1-RGO	481	89.16	68.14	118.0
AZO-2-RGO	477	120.8	112.06	192.44

[(a)] M_n is the molecular weight of AZO with the average number of carbon atoms supporting each AZO determined by TGA and XPS analysis.

High energy density of solar thermal storage.
In addition to storage stability, energy density of AZO/carbon nano-template is basically another core issue for solar thermal fuels. We determined energy density of AZO-RGO controlled by $\Delta H_{cis\text{-}trans}$ for per molecule by differential scanning calorimetry (DSC) using the method described in Ref.15 and discussed the result with the calculation data (Data S1†) from DFT based on a stable model.

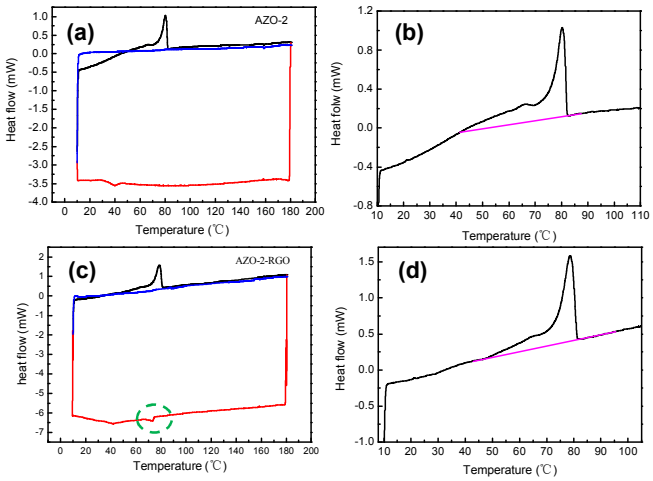

Fig.7 DSC traces of (a), (b) AZO-2 and (c), (d) AZO-2-RGO with the expanded view along with heating (black), cooling (red) and reheating (blue) segments.

Fig. 7 shows the DSC curves of AZO-2 and AZO-2-RGO powder in *cis*-rich photostationary states after irradiation by UV light. AZO-2 does not decompose at the full scanning temperature (0-180℃) according to TGA results. As shown in Fig. 7a and 7c, we found that AZO-2 and AZO-2-RGO nano-templates at the *cis*-rich metastable state exhibit a distinct exothermic heat flow over 42-86℃ (Fig. 7b) and 43-95℃ (Fig. 7d) in the first heating segment respectively, which is observed at a similar ranges of temperatures in other samples (AZO-1 and AZO-1-RGO) due to *cis*-to-*trans* isomerization. However, the exothermic heat flow disappeared in the reheating segment. It indicates that the exothermic heat flow in the first heating segment was stored energy from the light. In addition, compared with other samples without H-bond, AZO-2-RGO hybrid showed endothermic transition in the temperature-falling period approximately 75℃ by breaking a handful of H-bonds between neighboring AZO-2 on the surface of RGO (see dotted circle in Fig. 7c).

The exothermic heat flow of DSC data was used to calculate the enthalpy difference between the *cis* and *trans* isomers, which corresponds to the bulk gravimetric energy densities of 68 Wh kg^{-1} for AZO-1-RGO and 112 Wh kg^{-1} for AZO-2-RGO, while AZO-1 and AZO-2 with non-template only show much lower capacities of 42 and 40 Wh kg^{-1}, respectively (Table 2). This result is exciting in that the energy density of AZO-2-RGO is at least 1.6 time as that in previous studies (70 Wh kg^{-1})[14] and the period of storage is longer or comparable to other AZO/carbon composites shown in Fig. 8. Meanwhile, energy density is also confirmed by theoretical calculation using DFT (Table 2 and Data S1†), which shows that it is the same order magnitude to the experiment data.

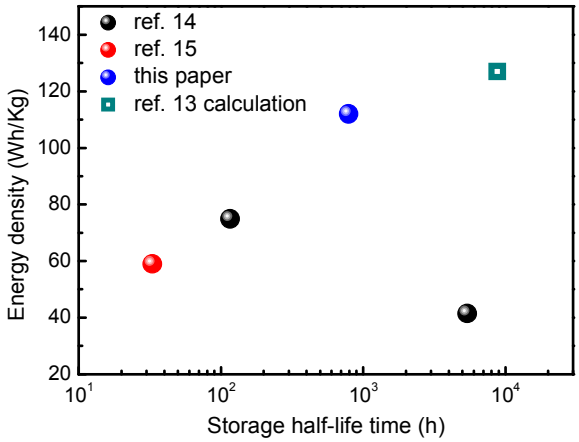

Fig.8 Energy densities and storage half-lifetime of solar thermal fuels using AZO/carbon nano-templates.

Here, we consider that the high capacity for solar thermal storage of AZO-2-RGO nano-template is mainly affected by the intermolecular H-bond and proximity-induced interaction controlled by high functionalization density and inter-planar bundling. Previous studies[3,13] indicated that the different numbers of intermolecular H-bonds between *trans*- and *cis*-AZO on the surface of RGO could significantly increase ΔH based on theoretical calculation. What is more, we believe that AZO-2-RGO shows intermolecular H-bonds and proximity-induced interaction not only between two neighboring AZO on the same nanosheets but also between two AZO on adjacent nanosheets by the combined effect of functional groups and packing interaction based on inter-planar bundling according to DFT calculation and XRD pattern, which could further observably increase the energy density for solar energy storage. However, it is worth noting that the energy density of AZO-1-RGO (without intermolecular H-bonds) is 2-fold relative to that of AZO-1 at the condition of bundling in solid state (Table 2). Besides, even though the degree of *cis*-to-*trans* transformation is 100%, the storage capacity (192 kJ mol^{-1}) of AZO-2-RGO (within intermolecular H-bonds, Fig. 7c) fuels is about 3.4-fold higher than that of AZO-2 molecule (non-template, 44 kJ mol^{-1}), showing great potential for high energy density solar thermal storage up to 112 Wh kg^{-1}, which is comparable to commercial soft-packing Li-ion batteries.

Conclusions

By utilizing an effective strategy, RGO nano-templates covalently functionalized with two light-active AZO molecules were attained for high energy density and long-term solar thermal storage. Intermolecular H-bonds and proximity-induced interaction with high functionalization density and packing interaction on account of inter-planar bundling in the solid state remarkably improve storage capacities and storage half-lifetime of the solar thermal fuels using AZO-RGO nano-templates. We have demonstrated that the novel solar thermal fuels exhibit a high energy density of solar thermal storage up to 112 Wh kg^{-1} in consistence with the theoretical calculation, simultaneous keeping a long-term storage with $\tau_{1/2}$ of 33 days. Furthermore, the nano-templates also show excellent cycling stability for 50 cycles irradiated by visible light, indicating the potential utilization for more than 4.5 years. The results presented here opens up a new pathway for high density solar thermal fuels based on a nano-template optimized by chemical structures and

molecular interaction, which could ultimately be utilized for large-scale solar thermal storage.

Acknowledgements

This work was financially supported by National Natural Science Funds for Distinguished Young Scholars (51425306), National Natural Science Foundation of China (Grant no. 51173127, 51273144, 51373116 and 513111129), and Natural Science Foundation of Tianjin City (No. 14JCZDJC37900) and Program for New Century Excellent Talents in University (NCET-13-0403).

Notes and references

[a] School of Materials Science and Engineering, Tianjin Key Laboratory of Composite and Functional Materials, Tianjin University, Tianjin 300072, China

[b] Beijing National Laboratory for Molecular Sciences, Key Laboratory of Organic Solids, Institute of Chemistry, Chinese Academy of Sciences, Beijing 100190, China.

† Email: weifeng@tju.edu.cn. Tel: +86-22-87402059 Fax: +86-22-27404724

Electronic Supplementary Information (ESI) available: [details of any supplementary information available should be included here]. See DOI: 10.1039/b000000x/

1. N. Armaroli and V. Balzani, *Angew. Chem. Int. Ed.,* 2007, **46**, 52.
2. T. R. Cook, D. K. Dogutan, S. Y. Reece, Y. Surendranath, T. S. Teets and D. G. Nocera, *Chem. Rev.*, 2010, **110**, 6474.
3. A. M. Kolpak and J. C. Grossman, *J. Chem. Phys.*, 2013, **138**, 034303.
4. Y. Kanai, V. Srinivasan, S. K. Meier, K. P. C. Vollhardt and J. C. Grossman, *Angew. Chem. Int. Ed.*, 2010, **49**, 8926.
5. K. Moth-Poulsen, D. Coso, K. Borjesson, N. Vinokurov, S. K. Meier, A. Majumdar, K. P. C. Vollhardt and R. A. Segalman, *Energ. Environ. Sci.*, 2012, **5**, 8534.
6. A. D. Dubonosov, Bren, V. A., Chernoivanov, V. A., *Russ. Chem. Rev.*, 2002, **71**, 914.
7. W. Feng, W. Luo and Y. Feng, *Nanoscale*, 2012, **4**, 6118.
8. P. G. van Rhee, R. S. M. Rikken, L. K. E. A. Abdelmohsen, J. C. Maan, R. J. M. Nolte, J. C. M. van Hest, P. C. M. Christianen and D. A. Wilson, *Nat Commun*, 2014, **5**.
9. H. Yamaguchi, Y. Kobayashi, R. Kobayashi, Y. Takashima, A. Hashidzume and A. Harada, *Nat Commun*, 2012, **3**, 603.
10. J. A. Krings, B. Vonhoren, P. Tegeder, V. Siozios, M. Peterlechner and B. J. Ravoo, *J. Mater. Chem. A*, 2014, **2**, 9587.
11. G. Lee, F. Araoka, K. Ishikawa, Y. Momoi, O. Haba, K. Yonetake and H. Takezoe, *Part. Part. Syst. Char.*, 2013, **30**, 847.
12. T. J. Kucharski, Y. Tian, S. Akbulatov and R. Boulatov, *Energ. Environ. Sci.*, 2011, **4**, 4449.
13. A. M. Kolpak and J. C. Grossman, *Nano Lett.*, 2011, **11**, 3156.
14. Y. Y. Feng, H. P. Liu, W. Luo, E. Z. Liu, N. Q. Zhao, K. Yoshino and W. Feng, *Sci Rep*, 2013, **3**, 3260.
15. T. J. Kucharski, N. Ferralis, A. M. Kolpak, J. O. Zheng, D. G. Nocera and J. C. Grossman, *Nat Chem*, 2014, **6**, 441.
16. V. Etacheri, R. Marom, R. Elazari, G. Salitra and D. Aurbach, *Energ. Environ. Sci.*, 2011, **4**, 3243.
17. Z. Wang, Z.-x. Li and Z. Liu, *J. Phys. Chem. C*, 2009, **113**, 3899.
18. X. Zhang, Y. Feng, D. Huang, Y. Li and W. Feng, *Carbon*, 2010, **48**, 3236.
19. X. Zhang, Y. Feng, P. Lv, Y. Shen and W. Feng, *Langmuir*, 2010, **26**, 18508.
20. D. C. Marcano, D. V. Kosynkin, J. M. Berlin, A. Sinitskii, Z. Sun, A. Slesarev, L. B. Alemany, W. Lu and J. M. Tour, *ACS Nano*, 2010, **4**, 4806.
21. J. R. Lomeda, C. D. Doyle, D. V. Kosynkin, W.-F. Hwang and J. M. Tour, *J. Am. Chem. Soc.*, 2008, **130**, 16201.
22. G. Kresse and D. Joubert, *Phys. Rev. B*, 1999, **59**, 1758.
23. J. P. Perdew, K. Burke and M. Ernzerhof, *Phys. Rev. Lett.*, 1996, **77**, 3865.
24. M. Methfessel and A. T. Paxton, *Phys. Rev. B*, 1989, **40**, 3616.
25. H. J. Monkhorst and J. D. Pack, *Phys. Rev. B*, 1976, **13**, 5188.
26. E. Bekyarova, M. E. Itkis, P. Ramesh, C. Berger, M. Sprinkle, W. A. de Heer and R. C. Haddon, *J. Am. Chem. Soc.*, 2009, **131**, 1336.
27. J. M. Englert, C. Dotzer, G. Yang, M. Schmid, C. Papp, J. M. Gottfried, H.-P. Steinrück, E. Spiecker, F. Hauke and A. Hirsch, *Nat Chem*, 2011, **3**, 279.
28. X. An, T. Simmons, R. Shah, C. Wolfe, K. M. Lewis, M. Washington, S. K. Nayak, S. Talapatra and S. Kar, *Nano Lett.*, 2010, **10**, 4295.
29. K. K. Pandey, *J. Appl. Polym. Sci.*, 1999, **71**, 1969.
30. R. I. Gearba, M. Lehmann, J. Levin, D. A. Ivanov, M. H. J. Koch, J. Barberá, M. G. Debije, J. Piris and Y. H. Geerts, *Adv. Mater.*, 2003, **15**, 1614.
31. L. Sharma, T. Matsuoka, T. Kimura and H. Matsuda, *Polym. Adv. Technol.*, 2002, **13**, 481.
32. H. Hu, Z. Zhao, W. Wan, Y. Gogotsi and J. Qiu, *Adv. Mater.*, 2013, **25**, 2219.
33. B. Zhang, Y. Zhang, C. Peng, M. Yu, L. Li, B. Deng, P. Hu, C. Fan, J. Li and Q. Huang, *Nanoscale*, 2012, **4**, 1742.
34. D. S. Yu, T. Kuila, N. H. Kim, P. Khanra and J. H. Lee, *Carbon*, 2013, **54**, 310.
35. M. Fang, K. Wang, H. Lu, Y. Yang and S. Nutt, *J. Mater. Chem.*, 2009, **19**, 7098.
36. K. N. Kudin, B. Ozbas, H. C. Schniepp, R. K. Prud'homme, I. A. Aksay and R. Car, *Nano Lett.*, 2007, **8**, 36.
37. D. Li, M. B. Muller, S. Gilje, R. B. Kaner and G. G. Wallace, *Nat Nano*, 2008, **3**, 101.
38. N. R. Neale, *Nat Chem*, 2014, **6**, 385.
39. A. A. Beharry, O. Sadovski and G. A. Woolley, *J. Am. Chem. Soc.*, 2011, **133**, 19684.
40. S. Samanta, A. A. Beharry, O. Sadovski, T. M. McCormick, A. Babalhavaeji, V. Tropepe and G. A. Woolley, *J. Am. Chem. Soc.*, 2013, **135**, 9777.
41. R. Siewertsen, H. Neumann, B. Buchheim-Stehn, R. Herges, C. Näther, F. Renth and F. Temps, *J. Am. Chem. Soc.*, 2009, **131**, 15594.
42. Y. Yang, R. P. Hughes and I. Aprahamian, *J. Am. Chem. Soc.*, 2012, 134, 15221.

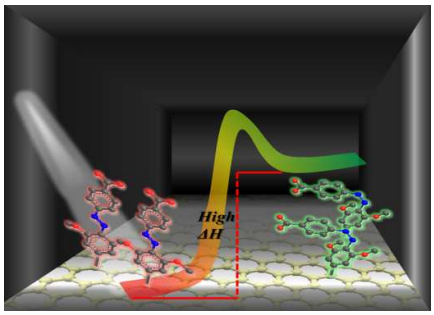

High functionalization density and inter-planar bundling interaction remarkably improve both storage capacity and lifetime for solar thermal fuels using azobenzene/graphene nano-template.